Journal of Alloys and Compounds 509 (2011) 546–550

Contents lists available at ScienceDirect

Journal of Alloys and Compounds

journal homepage: www.elsevier.com/locate/jallcom

Effect of Fe_2O_3 on Sm-doped ceria system solid electrolyte for IT-SOFCs

Yifeng Zheng, Ming Zhou, Lin Ge, Shujun Li, Han Chen, Lucun Guo*

College of Material Science and Engineering, Nanjing University of Technology, No.5 Xinmofan Road, Nanjing, Jiangsu 210009, PR China

ARTICLE INFO

Article history:
Received 10 July 2010
Received in revised form
15 September 2010
Accepted 18 September 2010
Available online 25 September 2010

Keywords:
Fuel cells
Sintering
Crystal structure
Ionic conduction
X-ray diffraction

ABSTRACT

The effect of Fe_2O_3 addition (0–2.5 mol%) on the densification, crystal structure, ionic conductivity, and aging behavior of $Ce_{0.8}Sm_{0.2}O_{1.9}$ (SDC) was studied. The addition of Fe_2O_3 promotes densification, reducing sintering temperature by ~100–150 °C. X-ray diffraction showed that these materials exhibit a fluorite structure; a second phase of Fe_2O_3 is identified when Fe_2O_3 content was ≥1.5 mol%. Impedance spectroscopy measurements indicated that SDC with 0.25 mol% Fe_2O_3 has the highest conductivity, about 10% higher than that of SDC at 700 °C. Conversely, a reduction in conductivity is observed in all samples after aging in air at 800 °C for 120 h. Because of the harmful effect of aging, conductivity rapidly decreases as Fe_2O_3 content in the samples exceeded 0.25 mol%. However, SDC with 0.25 mol% Fe_2O_3 shows the same magnitude of decrease in conductivity compared with that of SDC after aging. This indicates that SDC with 0.25 mol% Fe_2O_3 continues to present the best conductivity even after high-temperature aging.

1. Introduction

Solid oxide fuel cells (SOFCs) are important electrochemical devices that can directly convert chemical energy into electricity at high efficiency [1–5]. SOFCs have a wide range of applications in stationary power generation and transport. Traditional electrolytes based on yttria-stabilized zirconia are some of the most well-known electrolyte materials for SOFCs. However, their high operating temperature requirements (800–1000 °C) result in high costs, as well as physical and chemical degradation of component materials. An intensive investigation on reducing cell working temperatures to 600–800 °C has recently been conducted to enable the use of more inexpensive materials and expand the range of potential applications.

Doped ceria has been considered one of the most promising electrolyte materials for intermediate temperature SOFCs (IT-SOFCs) because of its high oxide ionic conductivity and good compatibility with electrodes [6–12]. The ionic conductivity of ceria-based electrolytes doped with various dopants (Sm^{3+}, Gd^{3+}, Y^{3+}, Ca^{2+}, etc) at different concentrations has been extensively investigated [13–15]. Sm^{3+} is one of the best dopants currently available for ceria-based solid electrolytes [13,16].

However, one of the main problems in ceria-based materials is poor sinterability. To reduce sintering temperatures, ultra-fine ceria-based powders are frequently used in physical and chemical methods, such as sol–gel synthesis, co-precipitation, chemical combustion vapor synthesis, and intensive mechanical milling [17–21]. Alternatively, sintering aids, such as CuO, Al_2O_3, MnO_2, ZnO and CoO [20,22–25], can be employed to promote densification. Nevertheless, these aids are relatively detrimental to the conductivity of ceria ceramics [20,22–25]. Fe_2O_3 has been reported not only as a good sintering aid, but also beneficial to the total conductivity of Gd^{3+}-doped ceria [26,27]. However, systematic studies on the Sm_2O_3–CeO_2 system with various ratios of Fe_2O_3 addition remain lacking.

The aging effects of solid electrolytes are also important in selecting optimum compositions for practical applications. The aging behavior of zirconia-based electrolytes, closely related to dopant type and concentrations, has been thoroughly examined [28,29]. Zhang et al. found that Y- or Gd-doped ceria ceramics undergo severe aging behavior, especially for the samples with high dopant content [30,31].

This study aims to investigate the effect of Fe_2O_3 on the sintering behavior, crystal structure, electrical properties, and aging behavior of the Sm-doped CeO_2 system ($Ce_{0.8}Sm_{0.2}O_{1.9}$). Special attention is paid to the optimum amount of Fe_2O_3 added.

2. Experimental

For the $(Ce_{0.8}Sm_{0.2}O_{1.9})_{1-x}+(Fe_2O_3)_x$ (x = 0, 0.0025, 0.005, 0.015, 0.025) mixtures, $Ce_{0.8}Sm_{0.2}O_{1.9}$ (SDC) powder was first prepared, to which Fe_2O_3 powder was added. CeO_2 (99.5% pure, Yixing Xinwei Leeshing Rare Earth Co., Ltd., China) and Sm_2O_3 (99.99% pure, Beijing Founde Star Science and Technology Co., Ltd., China) powders were used as starting materials for the preparation of $Ce_{0.8}Sm_{0.2}O_{1.9}$. The CeO_2 and Sm_2O_3 powders were thoroughly mixed with distilled water for 8 h, using zirconia (ZrO_2) milling media in a planetary mill. After being dried, the powders

* Corresponding author. Tel.: +86 25 83587261; fax: +86 25 83306152.
E-mail address: lc-guo@163.com (L. Guo).

0925-8388/$ – see front matter © 2010 Elsevier B.V. All rights reserved.
doi:10.1016/j.jallcom.2010.09.103

were ground and calcined in air at 1200 °C for 2 h. The calcined SDC and Fe_2O_3 (99.5% pure, Shanghai Chemical Reagent Plant, China) powders were mixed using zirconia balls in distilled water for 6 h, and then dried. The obtained powders were ground and pressed into pellets (13 mm diameter; 1 mm thickness), followed by cold-isostatic pressing at about 150 MPa. The powders were finally sintered in air at 1350–1600 °C for 2 h. The density of the sintered samples was determined based on the Archimedes principle and the dimension measurement method. High temperature aging in air at 800 °C for 120 h was performed on the sintered samples. The final sample is designated as "SDC-F*n*", where *n* is Fe_2O_3 mol% (or 100*x*). For example, $(Ce_{0.8}Sm_{0.2}O_{1.9})_{1-x} + (Fe_2O_3)_x$ ($x = 0.0025$) is designated as SDC-F0.25.

The crystal structures of the samples (again ground to powder for measurement) at room temperature were determined by XRD using an ARL X'TRA diffractometer and Cu Kα radiation. The diffractometer was operated at 40 kV and 35 mA at a scanning range of 20–80°, with a step size of 0.02°.

To prepare samples for the ionic conductivity measurements, silver paste was painted on both sides of the specimens followed by baking at 700 °C for 10 min. The AC impedance spectra of the samples were measured as a function of temperature (300–800 °C) in air using an impedance analyzer (PARSTAT 2273) in the frequency range from 0.1 Hz to 1 MHz. Data were collected using a SMART program and fitted to the corresponding equivalent circuits with the ZSimpWin software.

3. Results and discussion

3.1. Shrinkage and densification

Fig. 1 shows the linear shrinkage curves of SDC with different Fe_2O_3 contents. The difference in sintering behavior between Fe_2O_3-added samples and SDC is relatively evident from the figure. The addition of small amounts of Fe_2O_3 significantly reduces the temperature of maximum shrinkage, indicating good effect in promoting the sintering behavior of SDC. An enhancement in sintering procedure is observed with Fe_2O_3 content (x) of 0.0025–0.015. Moreover, a further increase in Fe_2O_3 content ($x = 0.025$) also increases the effects on shrinkage. The modified systems to which Fe_2O_3 was added achieve a certain shrinkage degree at a temperature ~100–150 °C lower compared with SDC.

The variation in relative density with respect to sintering temperature for all the samples is shown in Fig. 2. The samples with Fe_2O_3 achieve the peak value (~95%) at 1500 or 1450 °C, whereas relative density is only 76% for SDC at 1500 °C. The addition of Fe_2O_3 strongly promotes the densification rate of SDC probably because viscous flow sintering occurred in the Fe-doped ceria system. In this study, the optimum sintering temperatures for SDC, SDC-F0.25, SDC-F0.5, SDC-F1.5, and SDC-F2.5 are 1600, 1500, 1500, 1500, and 1450 °C, respectively.

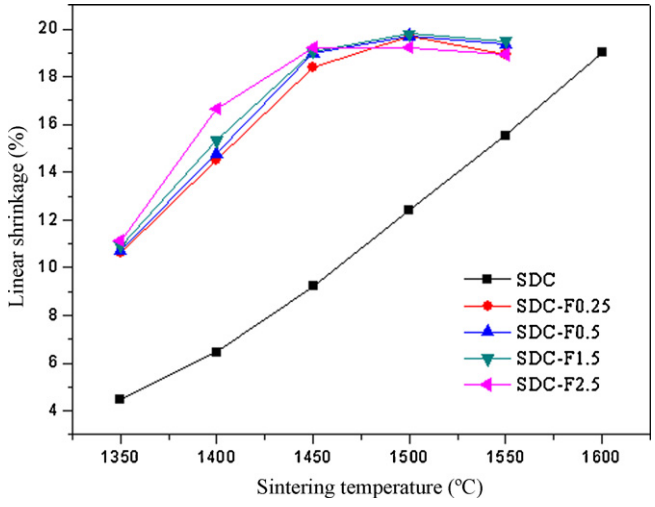

Fig. 1. Linear shrinkage vs. sintering temperature for SDC with different Fe_2O_3 contents.

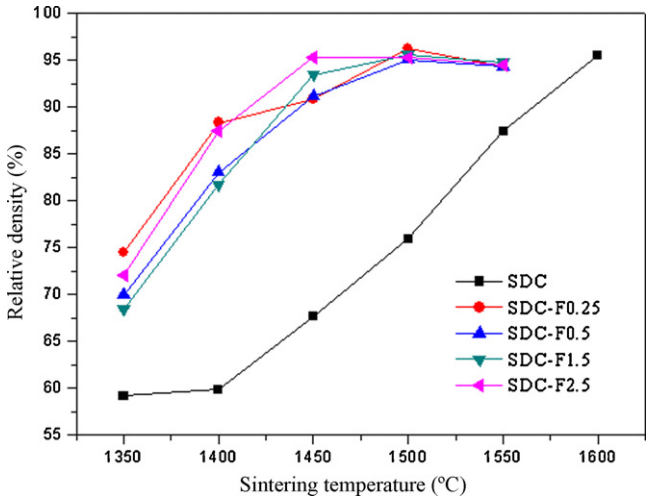

Fig. 2. Relative density vs. sintering temperature for SDC with different Fe_2O_3 contents.

3.2. Phase composition and crystal structure

The XRD patterns of the sintered samples are shown in Fig. 3. The samples exhibit all the major peaks of a fluorite structure. Small additional Fe_2O_3 peaks appear when the content (x) of Fe_2O_3 reaches 0.015, indicating that Fe_2O_3 has limited solubility in SDC. Lattice parameters of each sample were obtained by fitting the peak data of the ceria phase using the Jade software. The relationship between lattice parameters and Fe_2O_3 content is shown in Fig. 4. The lattice parameters decrease linearly with increasing Fe_2O_3 concentration from 0.5432 nm to 0.5417 nm when Fe_2O_3 content (x) is lower than 0.015; the parameters remain almost constant with continued addition. Because Fe^{3+} has a radius (0.078 nm) much smaller than that of Ce^{4+} (0.097 nm) [32], substituting Fe^{3+} for Ce^{4+} can induce the variation in lattice parameters. The minimum lattice parameter at around $x = 0.015$ indicates that Fe_2O_3 almost dissolves into CeO_2 below this content. Hence, the transformation of lattice parameters, as shown in Fig. 4, demonstrates that the substitutional solid solubility limit of Fe_2O_3 in CeO_2 is around $x = 0.015$ (1.5 mol%) in this study. The solubility of Fe^{3+} into ceria compound is reportedly small (less than 1.0 at.%) at room temperature to 1500 °C [33]. However, Ref. [26] showed that about 2.5 mol% Fe_2O_3 can dissolve into $Ce_{0.8}Gd_{0.2}O_{1.9}$ ceramics. Moreover, Matovic et al. reported that

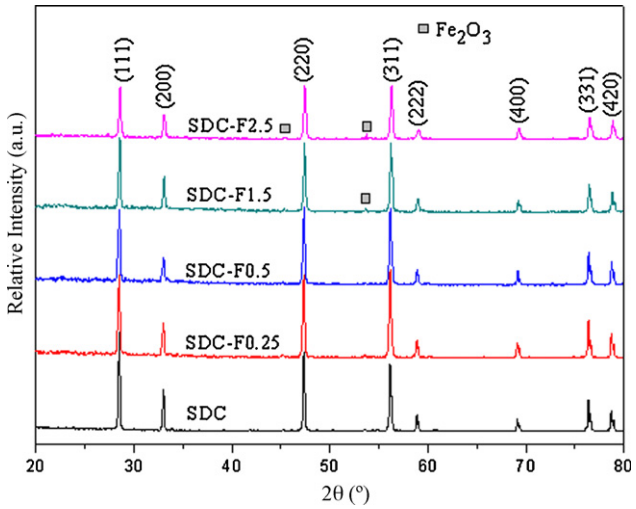

Fig. 3. XRD patterns of SDC with different Fe_2O_3 contents.

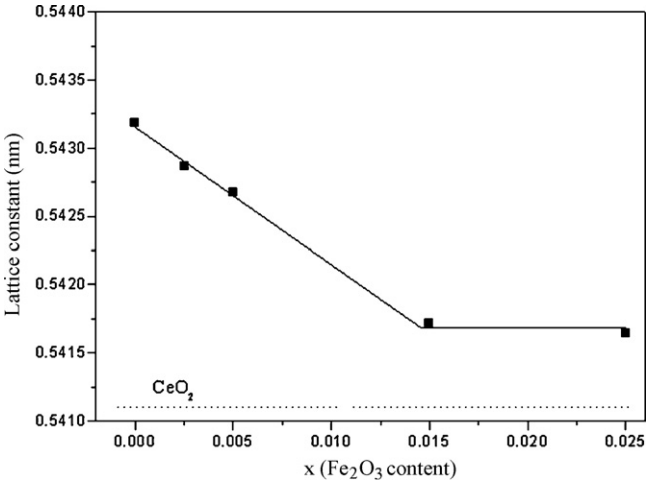

Fig. 4. Lattice parameters derived from the XRD patterns vs. Fe_2O_3 contents.

the limit of solubility of Fe in CeO_2 prepared from self-propagating room temperature synthesis is in the range of 5–7.5 wt.% [34]. The difference in Fe solubility in ceria may be attributed to the prepared technique.

3.3. Electrical properties

A representative Nyquist impedance spectrum and equivalent circuit model of SDC at 300 °C distinguishing three separate regions are shown in Fig. 5. The high frequency part is attributed to the grain interior (bulk) response; the medium frequency semicircle corresponds to grain boundary; and the low frequency arc represents the sample-electrode connection. The contributions of these three parts can be clearly identified in the impedance spectra measured below 500 °C in air in this experiment. The impedance spectra were fitted to the equivalent circuit containing three Resistance-Constant Phase Element (R-CPE) subcircuits in series (Fig. 5). These circuits are used only to obtain the best fit and adequately determine the electrolyte resistance, and not to explain the kinetics of redox reactions at the electrodes. At high measurement temperatures, the time constants decrease and the arcs shift to higher frequencies. Therefore, only parts of the arcs appear in the impedance spectrum because of the limited frequency range of the equipment. The bulk and grain boundary arcs are associated with the capacitances in the pF and nF ranges, respectively, determined from $2\pi f_{max}RC = 1$, where f_{max} is the applied frequency at arc maximum and R is the arc magnitude [8]. The total resistance of electrolyte is given by

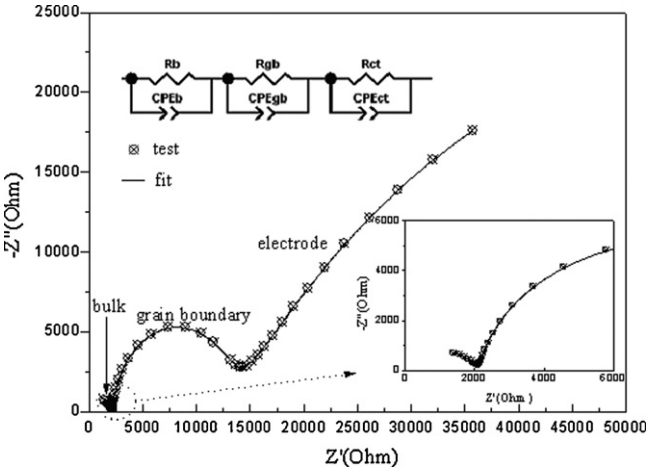

Fig. 5. Impedance spectra obtained for SDC at 300 °C and the equivalent circuit model used for spectra interpretation.

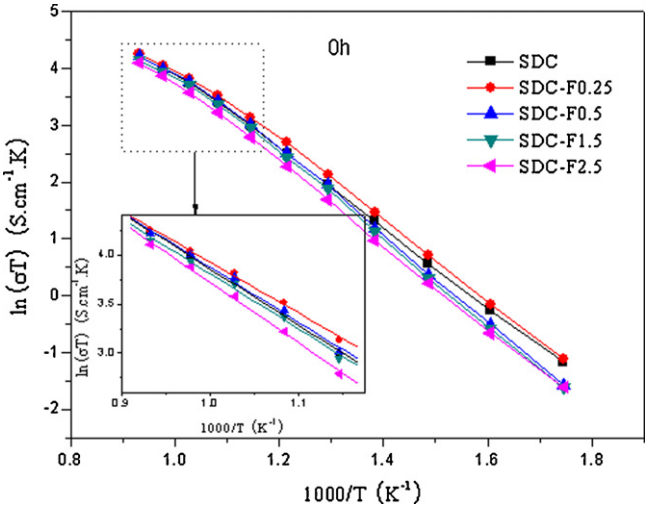

Fig. 6. Temperature dependence of the total conductivities of SDC at different Fe_2O_3 contents.

$$R_t = R_b + R_{gb} \quad (1)$$

where R_b is bulk resistance and R_{gb} is grain boundary resistance. They are both obtained by fitting the impedance data. The total conductivity at different temperatures can be obtained using the equation

$$\sigma = \frac{L}{SR_t} \quad (2)$$

where L and S represent the sample thickness and the electrode area of the sample surface, respectively. The measured conductivity data are analyzed with the Arrhenius equation

$$\sigma = \frac{A}{T}\exp\left(-\frac{E}{kT}\right) \quad (3)$$

where E is the activation energy for ionic migration, k is the Boltzman's constant, T represents the absolute temperature, and A denotes the pre-exponential factor (constant at a certain temperature range).

Fig. 6 shows the relationships among the total conductivity levels of the samples with different Fe_2O_3 contents at temperatures ranging from 300 to 800 °C. The total conductivity is affected by the addition of Fe_2O_3; the conductivity increases and then decreases with Fe_2O_3 content. The difference in conductivity is smaller in the high temperature region than that in the low temperature region for all the samples. SDC-F0.25 shows higher conductivity than does SDC in all temperatures, about 10% higher at 700 °C. A slightly higher conductivity is observed for SDC-F0.5 at 600–800 °C compared with that for SDC. However, both SDC-F1.5 and SDC-F2.5 cannot improve SDC conductivity because the formation of second-phase Fe_2O_3 diminishes electrochemical property.

The predominant constituent of the grain boundary impurities in ceria-based solid solutions is SiO_2. In this study, the grain boundary effect for all the samples cannot be detected above 500 °C because of spectra of inductances generated within the experimental apparatus. These results are in good agreement with those in Refs. [6,35]. However, the grain boundary effect dominates the total conductivity up to 1000 °C for impure ceria-based materials. Therefore, because Fe_2O_3 is a grain boundary scavenger of SiO_2 impurity [26], Fe_2O_3 can be beneficial to the electrical property of SDC electrolyte. The Fe^{3+} doping action is the same as that of Sm^{3+} ions, as described in Eq. (4), but the lattice mismatch between

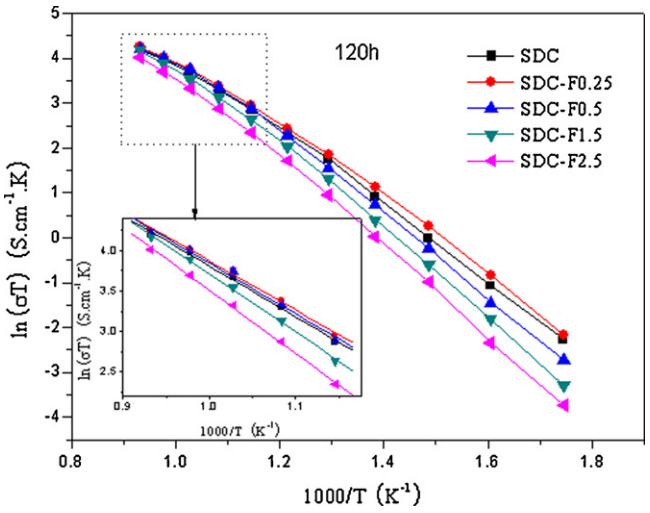

Fig. 7. Temperature dependence of the total conductivities of SDC with different Fe_2O_3 contents after aging at 800 °C for 120 h.

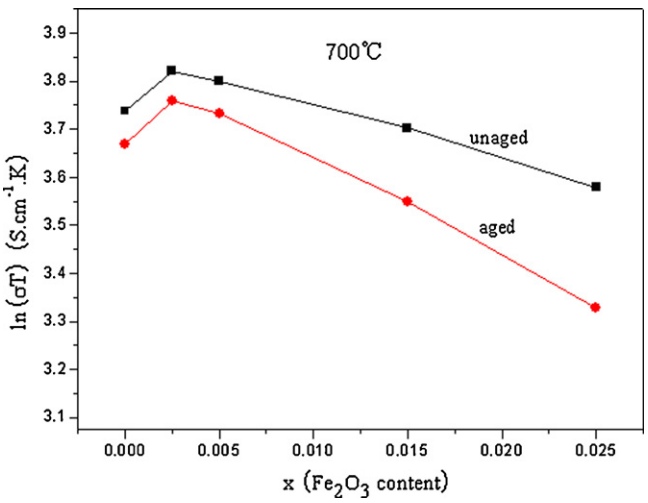

Fig. 8. Total conductivities of samples measured at 700 °C after aging at 800 °C for 0 and 120 h in air vs. Fe_2O_3 content.

Fe^{3+} (0.078 nm) and Ce^{4+} (0.097 nm) is higher than that between Sm^{3+} (0.1079 nm) and Ce^{4+} (0.097 nm). Furthermore, the electrostatic attraction between Fe'_{Ce} and $V_O^{\bullet\bullet}$ is stronger than that between Sm'_{Ce} and $V_O^{\bullet\bullet}$. Therefore, the defect association between Fe'_{Ce} and $V_O^{\bullet\bullet}$ is expected to be more easily determinable than that between Sm'_{Ce} and $V_O^{\bullet\bullet}$.

$$Sm_2O_3 \xrightarrow{2CeO_2} 2Sm'_{Ce} + 3O_O^{\times} + V_O^{\bullet\bullet} \quad (4)$$

The dissolution of Fe will deplete the concentration of free $V_O^{\bullet\bullet}$ produced by Sm doping because each Fe^{3+} ion would attract one $V_O^{\bullet\bullet}$ to form a defect complex (e.g., $Fe'_{Ce}V''_O$) [27,36], thereby decreasing conductivity. For the samples of $(Ce_{0.8}Sm_{0.2}O_{1.9})_{1-x} + (Fe_2O_3)_x$, the addition of Fe_2O_3 to SDC may produce two opposite effects. On one hand, SiO_2 impurity in SDC will be scavenged by appropriate Fe_2O_3 content, increasing conductivity. On the other hand, Fe^{3+} ions will attract $V_O^{\bullet\bullet}$ to form the defect complex, which decreases conductivity. When the Fe_2O_3 content (x) is below 0.005, the first effect might be stronger than the second, resulting in higher conductivity. However, when the dopant content (x) is above 0.005, the second effect might become stronger than the first, leading to decrease conductivity. The second-phase Fe_2O_3 also deteriorates the electrochemical properties when $x \geq 0.015$. Therefore, to obtain an electrolyte with high conductivity, the ratio of Fe_2O_3 to SDC should be appropriately tailored. In this study, the optimum Fe_2O_3 content to be added is about 0.0025.

3.4. Aging effects

Fig. 7 shows the temperature dependence of the total conductivity of SDC with different Fe_2O_3 contents after they were maintained at 800 °C for 120 h. Similarly, higher conductivity is observed for SDC-F0.25 in the entire temperature range and for SDC-F0.5 in the temperature range of 600–800 °C compared with SDC after thermal aging. This indicates that SDC with Fe_2O_3 has higher conductivity after prolonged heating.

The operating temperature range of IT-SOFCs is at 600–800 °C; thus, the range in this study was mainly confined between 600 and 800 °C. The selected total conductivities of unaged and aged samples measured at 700 °C are shown in Fig. 8. It can be seen that there is a decrease in conductivity in all samples as a function of time at 800 °C. The conductivity rapidly decreases as Fe_2O_3 content (x) exceeds 0.0025 for aged samples. Interestingly, the conductivities of SDC-F0.25 and SDC decrease at the same magnitude after aging. Therefore, SDC-0.25 still registers the best conductivity after high-temperature aging. The optimal Fe_2O_3 content (x) is 0.0025 before and after heating.

The activation energies of unaged and aged samples within 600–800 °C as a function of Fe_2O_3 content are shown in Fig. 9. Before and after aging, the activation energies of the SDC-F0.25 sample are lower than those of SDC, consistent with the total conductivity results shown in Figs. 6 and 7. The activation energies of the samples decrease with Fe_2O_3 substitution up to a minimum of $x = 0.0025$. The changes in activation energy with composition seem to be correlated with compositional variations in conductivity: the maximum value of total ionic conductivity corresponds to the minimum activation energy in agreement with the compensation rule of Meyer–Neldel [37].

Fig. 10 shows the XRD patterns of SDC with different Fe_2O_3 contents after aging at 800 °C for 120 h. No significant difference exists in the crystal phase between the aged (Fig. 10) and unaged (Fig. 3) samples, indicating that no significant change in composition or phase of the samples is caused by prolonged heating—a result in good agreement with Ref. [30]. SEM observations cannot provide appreciable variation in microstructures as a result of aging. According to Zhang [30], the formation of microdomains

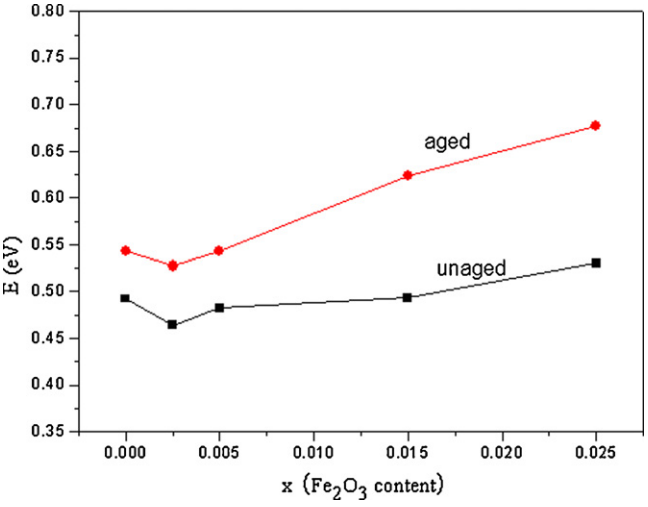

Fig. 9. Activation energies of conduction of samples measured at 600–800 °C after aging at 800 °C for 0 and 120 h in air vs. Fe_2O_3 content.

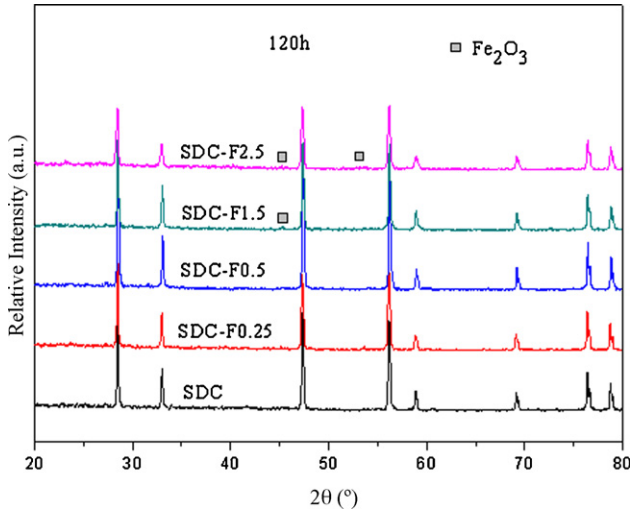

Fig. 10. XRD patterns of SDC with different Fe_2O_3 contents after aging at 800 °C for 120 h.

is considered the most possible contribution to aging behavior in doped ceria. The mechanisms underlying the effect of Fe_2O_3 on the aging behavior of SDC will be investigated further.

4. Conclusions

The densification, crystal structure, ionic conductivity, and aging behavior of SDC with the addition of Fe_2O_3 (0–2.5 mol%) were investigated. The addition of Fe_2O_3 reduces the sintering temperature of SDC by ~100–150 °C. A second-phase Fe_2O_3 is formed at an Fe_2O_3 content of ≥1.5 mol%. Impedance spectroscopy measurements indicated that the conductivity of SDC can be improved with the addition of appropriate amounts of Fe_2O_3. A reduction in total conductivity is observed in all the samples after aging in air at 800 °C for 120 h. However, the SDC with appropriate amounts of Fe_2O_3 also show higher conductivity after thermal aging. XRD showed that no significant change in composition or phase of the samples is caused by prolonged heating. In this study, the SDC with 0.25 mol% Fe_2O_3 [$(Ce_{0.8}Sm_{0.2}O_{1.9})_{0.9975} + (Fe_2O_3)_{0.0025}$] exhibits the highest conductivity and the lowest activation energy before and after high-temperature aging.

Acknowledgements

This work was financially supported by the Graduate Science and Technology Innovation Foundation of Jiangsu (CX10B_161Z) and the Science and Technology Pillar Program (Industry) of Jiangsu Province (BE2009169). We also acknowledge the support of Jiangsu Provincial Key Laboratory of Inorganic and Composite Materials.

References

[1] J.S. Ahn, S. Omar, H. Yoon, J.C. Nino, E.D. Wachsman, J. Power Sources 195 (2010) 2131–2135.
[2] H.T. Lim, A.V. Virkar, J. Power Sources 192 (2009) 267–278.
[3] S. Tao, J.T.S. Irvine, J.A. Kilner, Adv. Mater. 17 (2005) 1734–1737.
[4] C.M. Lapa, D.P.F. Souza, F.M.L. Figueiredo, F.M.B. Marques, Int. J. Hydrogen Energy 35 (2010) 2737–2741.
[5] H.P. Ding, X.J. Xue, J. Alloys Compd. 496 (2010) 683–686.
[6] B.C.H. Steele, Solid State Ionics 129 (2000) 95–110.
[7] S.A. Li, Z.C. Li, B. Bergman, J. Alloys Compd. 492 (2010) 392–395.
[8] S. Kuharuangrong, J. Power Sources 171 (2007) 506–510.
[9] Y.M. Kim, P.K. Lohsoontorn, J. Bae, J. Power Sources 195 (2010) 6420–6427.
[10] Z.G. Tang, Q.Z. Lin, B.E. Mellander, B. Zhu, Int. J. Hydrogen Energy 35 (2010) 2970–2975.
[11] C.M. Lapa, D.P. Ferreira de Souza, F.M.L. Figueiredo, F.M.B. Marques, J. Power Sources 187 (2009) 204–208.
[12] R. Raza, X.D. Wang, Y. Ma, B. Zhu, J. Power Sources 195 (2010) 6491–6495.
[13] H. Yahiro, K. Eguchi, H. Arai, Solid State Ionics 36 (1989) 71–75.
[14] L.D. Jadhav, M.G. Chourashiya, A.P. Jamale, A.U. Chavan, S.P. Patil, J. Alloys Compd. 506 (2010) 739–744.
[15] S. Ramesh, V.P. Kumar, P. Kistaiah, C.V. Reddy, Solid State Ionics 181 (2010) 86–91.
[16] K. Eguchi, T. Setoguchi, T. Inoue, H. Arai, Solid State Ionics 52 (1992) 165– 172.
[17] A. Moure, J. Tartaj, C. Moure, J. Eur. Ceram. Soc. 29 (2009) 2559–2565.
[18] J.V. Herle, T. Horita, T. Kawada, N. Sakai, H. Yokokawa, M. Dokiya, Solid State Ionics 86–88 (1996) 1255–1258.
[19] J. Li, T. Ikegami, T. Mori, Acta Mater. 52 (2004) 2221–2228.
[20] C. Kleinlogel, L.J. Gauckler, Solid State Ionics 135 (2000) 567–573.
[21] T.S. Zhang, J. Ma, Y.J. Leng, S.H. Chan, P. Hing, J.A. Kilner, Solid State Ionics 168 (2004) 187–195.
[22] X. Zhang, C.D. Petit, S. Yick, M. Robertson, O. Kesler, R. Maric, D. Ghosh, J. Power Sources 162 (2006) 480–485.
[23] Y.J. Kang, G.M. Choi, Solid State Ionics 180 (2009) 886–890.
[24] T.S. Zhang, L.B. Kong, Z.Q. Zeng, H.T. Huang, P. Hing, Z.T. Xia, J. Kilner, J. Solid State Electrochem. 7 (2003) 348–354.
[25] L. Gao, M. Zhou, Y.F. Zheng, H.T. Gu, H. Chen, L.C. Guo, J. Power Sources 195 (2010) 3130–3134.
[26] T.S. Zhang, J. Ma, L.B. Kong, S.H. Chan, P. Hing, J.A. Kilner, Solid State Ionics 167 (2004) 203–207.
[27] Q. Dong, Z.H. Du, T.S. Zhang, J. Lu, X.C. Song, J. Ma, Int. J. Hydrogen Energy 34 (2009) 7903–7909.
[28] A.N. Vlasov, M.V. Perfilier, Solid State Ionics 25 (1987) 245–253.
[29] S.P.S. Badwal, Solid State Ionics 52 (1992) 23–32.
[30] T.S. Zhang, J. Ma, L.B. Kong, S.H. Chan, J.A. Kilner, Solid State Ionics 170 (2004) 209–217.
[31] T.S. Zhang, J. Ma, H.T. Huang, P. Hing, Z.T. Xia, S.H. Chan, J.A. Kilner, Solid State Sci. 5 (2003) 1505–1511.
[32] R.D. Shannon, Acta Crystallogr. A32 (1976) 751–767.
[33] T. Zhang, P. Hing, H. Huang, J. Kilner, J. Eur. Ceram. Sci. 21 (2001) 2221–2228.
[34] B. Matovic, Z.D. Mitrovic, M. Radovic, Z. Brankovic, G. Brankovic, S. Boskovic, Z.V. Popovic, J. Power Sources 193 (2009) 146–149.
[35] R.O. Fuentes, R.T. Baker, Int. J. Hydrogen Energy 33 (2008) 3480–3484.
[36] L.P. Li, G.S. Li, J. Xiang, R.L. Smith Jr., H. Inomata, Chem. Mater. 15 (2003) 889–898.
[37] W. Meyer, H. Neldel, Z. Tech. Phys. 12 (1937) 588–593.